



Redefinition of beraunite, $\text{Fe}_6^{3+}(\text{PO}_4)_4\text{O}(\text{OH})_4 \cdot 6\text{H}_2\text{O}$, and discreditation of the name *eleonorite*: a re-investigation of type material from the Hrbek Mine (Czech Republic)

Luboš Vrtiška^{1,2}, Jaromír Tvrđý², Jakub Plášil³, Jiří Sejkora¹, Radek Škoda², Nikita V. Chukanov⁴,
Andreas Massanek⁵, Jan Filip⁶, Zdeněk Dolníček¹, and František Veselovský⁷

¹Department of Mineralogy and Petrology, National Museum,
Cirkusová 1740, 19300 Prague 9, Czech Republic

²Department of Geological Sciences, Faculty of Science, Masaryk University,
Kotlářská 2, 61137 Brno, Czech Republic

³Institute of Physics ASCR, v.v.i., Na Slovance 2, 18221 Prague 8, Czech Republic

⁴Institute of Problems of Chemical Physics, Russian Academy of Sciences,
Chernogolovka, Moscow region, 142432, Russia

⁵Geoscientific Collections, Technische Universität Bergakademie Freiberg,
A.-G.-Werner-Bau, Brennhausgasse 14, 09596 Freiberg, Germany

⁶Regional Centre of Advanced Technologies and Materials, Czech Advanced Technology and Research
Institute, Palacký University, Šlechtitelů 27, 78371 Olomouc, Czech Republic

⁷Czech Geological Survey, Klárov 131/3, 118 21 Prague 1, Czech Republic

Correspondence: Luboš Vrtiška (lubos.vrtiska@nm.cz)

Received: 4 January 2022 – Revised: 15 February 2022 – Accepted: 18 February 2022 – Published: 12 April 2022

Abstract. Re-investigation of the type material of beraunite from the Hrbek Mine, Svatá Dobrotivá, Czech Republic, proved the identity of beraunite and *eleonorite*. Based on this study, the mineral *eleonorite* was discredited, and the ideal formula of beraunite was redefined from $\text{Fe}^{2+}\text{Fe}_5^{3+}(\text{PO}_4)_4(\text{OH})_5 \cdot 6\text{H}_2\text{O}$ to $\text{Fe}_6^{3+}(\text{PO}_4)_4\text{O}(\text{OH})_4 \cdot 6\text{H}_2\text{O}$. Beraunite from Hrbek Mine usually forms prismatic crystals flattened on {100}; elongated along *b* axis, striated on {100} || *b*, up to $0.2 \times 0.5 \times 3$ mm, often in radial clusters up to 6 mm in size in association with black goethite, olive-green to dark green dufrénite and yellow to orange cacoxenite. Beraunite is hyacinth red, dark red, or red-brown and has a light orange-red streak; crystals are translucent, with a vitreous luster. The symmetry of the structure was found to be lower (*Cc*) than reported in the past (*C2/c*); this has been proven by the crystal structure refinement, $R_{\text{obs}} = 2.7\%$ for *Cc* and $\sim 8\%$ for *C2/m*. Refined unit-cell parameters obtained from powder X-ray diffraction data of the original material of Friedrich August Breithaupt are $a = 20.653(2)$, $b = 5.1433(6)$, $c = 19.241(2)$ Å, $\beta = 93.560(9)^\circ$, and $V = 2039.9(2)$ Å³. Calculated density is 2.961 g cm^{-3} . Beraunite is optically biaxial (+), $\alpha = 1.768(2)$, $\beta = 1.781(3)$, $\gamma > 1.805$, $2V_{\text{meas}} = 69(4)^\circ$, and $2V_{\text{calc}}$ is not possible to calculate. Dispersion of optical axes is strong, $r > v$. The orientation is $Y = b$, $X \approx a$, and $Z \approx c$. Pleochroism is strong; Z (brown-red) $\gg Y > X$ (both brownish yellow). The empirical formula of the original beraunite sample calculated on the basis of $P = 4$ apfu is $(\text{Fe}_{3.76}^{3+}\text{Al}_{0.15}\text{Zn}_{0.01})_{5.92}(\text{PO}_4)_{4.00}\text{O}_{0.99}(\text{OH})_{3.77} \cdot 6\text{H}_2\text{O}$. The ⁵⁷Fe Mössbauer spectrum of beraunite neotype (National Museum, Prague) from type locality implies that all iron atoms in beraunite structure are exclusively trivalent, located at the *M* site with different next-nearest-neighbor configurations. There is no spectral evidence for Fe^{2+} or iron in some impurities (e.g., *limonite*).

1 Introduction

Basic iron phosphates of the transition metals (particularly those of Fe^{2+} , Fe^{3+} , Mn^{2+} , and Mn^{3+}) belong to the most perplexing substances in the mineral kingdom (Moore, 1969, 1970). Although they have been known for a long time and have a relatively simple chemical composition, their detailed study brings a number of surprises. A typical example is beraunite, known in science for almost 2 centuries. The study of the original material of beraunite from the type locality Hrbek Mine, Svatá Dobrotivá, Czech Republic, deposited in collections of Technische Universität Bergakademie Freiberg (Germany) and National Museum Prague (Czech Republic), proved the identity of the minerals beraunite and *eleonorite* ($\text{Fe}_6^{3+}(\text{PO}_4)_4\text{O}(\text{OH})_4 \cdot 6\text{H}_2\text{O}$). Because the name beraunite (Breithaupt, 1840, 1841) has a priority, we consider the name eleonorite (Nies, 1877, 1880; Chukanov et al., 2017) to be redundant and proposed to abolish it. The proposal 21D approved by the CNMNC of the IMA discredited eleonorite and accepted the formula of beraunite as $\text{Fe}_6^{3+}(\text{PO}_4)_4\text{O}(\text{OH})_4 \cdot 6\text{H}_2\text{O}$. A structurally related mixed-valence iron phosphate $\text{Fe}^{2+}\text{Fe}_5^{3+}(\text{PO}_4)_4(\text{OH})_5 \cdot 6\text{H}_2\text{O}$ has been approved as a new mineral ferroberaunite (IMA no. 2021-036; Tvrđý et al., 2021).

2 Occurrence

The type locality of beraunite is the long-abandoned mine Hrbek in the Central Bohemian Region, Czech Republic. Hrbek was one of the small mines supplying Ordovician sedimentary iron ore (*limonite* and hematite) to the ironworks in Svatá Dobrotivá (formerly St. Benigna) in the manor of Zbiroh (formerly Zbirow). These iron ores are geologically part of the Teplá–Barrandian unit of the Bohemian Massif. Major mineralogical discoveries come from the peak period of mining in the early 19th century. In fissures of the limonite ore, beraunite occurred alone or accompanied by other phosphates, such as cacoxenite (described as a new mineral species from there by Steinmann, 1826), dufrénite, strengite, wavellite, and delvauxite (Velebil et al., 2018). The name beraunite is derived from the district town of Beroun, from its old German version, *Beraun* (Breithaupt, 1840). The type locality provided a relatively large number of specimens at the time, which became part of many historical mineralogical collections. Despite a number of publications on beraunite and beraunite-related minerals, the type material has not yet been the subject of modern research, surprisingly.

An original Breithaupt's specimen of beraunite from Hrbek Mine (labeled as FR) was recently discovered in the Mineralogical Collection of the TU Bergakademie Freiberg under the inventory number 21519. The aforementioned no. 21359 (e.g., Anthony et al., 2000) is incorrect, as it refers to another piece from Hrbek included later in the collections by Friedrich Kolbeck (in 1928). As it was not possible



Figure 1. Original specimen of beraunite, in paragenesis with cacoxenite and wavellite. Hrbek mine, Svatá Dobrotivá (St. Benigna), Beroun, Bohemia, Czech Republic. Mineralogical Collection of the TU Bergakademie Freiberg, inv. no. 21519 (sample FR). 10.5 × 5 cm. Photo A. Massanek.

to obtain enough sample for Mössbauer spectroscopy from the original Breithaupt's material, another specimen from the type locality was included in our study, too. This neotype specimen (labeled as NM) is stored in the Mineralogical Collection of the National Museum in Prague under the number PIN 18943 and comes from the original finds in the 19th century (Bořický, 1867).

3 Appearance, physical properties, and optical data

The original beraunite specimen 10.5 × 5 × 1.5 cm in size (sample FR; Fig. 1) was given to the then curator and professor of mineralogy at the Bergakademie Freiberg (Freiberg Mining Academy), Friedrich August Breithaupt, from the *Geheimer Kabinettsrath* (Privy Council member) Gottlieb L. Heyer in 1831 (Fig. 2). Breithaupt recognized that an unknown mineral was present on the specimen and labeled it as *a red radial mineral* accompanied by cacoxenite and *lasionite* (wavellite). Due to the ambiguous mineral designation on the label, the piece was later classified under cacoxenite, so that it has long remained unrecognized as a type material for beraunite in the mineralogical collections.

The reddish beraunite crystals occur mainly as radial to coarse-grained fissure fillings on massive brown iron ore. Almost only cleavage surfaces can be seen on the approximately 1–2 mm large crystals (Fig. 3). The associated minerals are dark brown to golden-yellow cacoxenite and reddish wavellite.

Studied beraunite from the collection of the National Museum in Prague (sample NM) forms rich crystal aggregates on fissures and encrusting cavities in massive limonite (sample size 8 × 5 cm; Fig. 4). Beraunite usually forms prismatic crystals flattened on {100}, elongated along the *b* axis, striated on {100} || *b*, up to 0.2 × 0.5 × 3 mm, often in radial

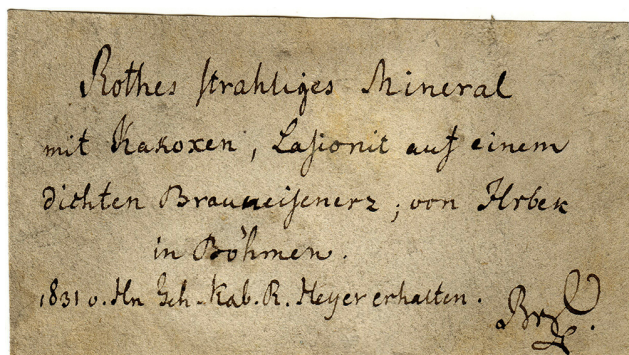


Figure 2. Original label of the original beraunite specimen written by Friedrich August Breithaupt in 1831. “Rothes strahliges Mineral mit Kakoxen, Lasionit auf einem dichten Brauneisenerz; von Hrbek in Böhmen. 1831 v. [von] Hn [Herrn] Geh. Kab. R. [Geheimen Kabinettsrath] Heyer erhalten. Br [Breithaupt].”



Figure 3. Dark red crystalline aggregates of beraunite associated with brown to yellow cacoxenite. Mineralogical Collection of the TU Bergakademie Freiberg, inv. no. 21519 (original beraunite specimen; sample FR). FOV 15 mm. Photo A. Massanek.

clusters up to 6 mm in size in association with black goethite, olive-green to dark green dufrénite, and yellow to orange cacoxenite (Fig. 5).

Beraunite is hyacinth red, dark red, or red-brown and has a light orange-red streak. Crystals are translucent, with a vitreous luster. The mineral is brittle, with a Mohs hardness of 3. Cleavage is perfect on (100). It dissolves well in HCl (35%), dissolves slowly in H₃PO₄ (85%), and does not dissolve in HNO₃ (65%; room temperature; 24 h observation, 1 mm fragments; sample NM).

Density measured by the flotation method using two different mixtures of liquids (diiodomethane and acetone; 1,1,2,2-tetrabromoethane and dioxane) and the Mohr–Westphal scale is 2.88 (± 0.01) g cm⁻³ (sample FR) and 2.91 (± 0.01) g cm⁻³ (sample NM). The density calculated from the empirical formula and unit-cell parameters from single-crystal diffraction is 2.961 g cm⁻³.

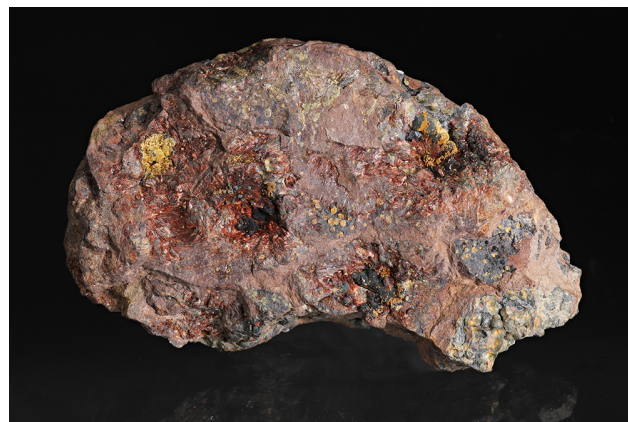


Figure 4. Neotype specimen of beraunite from the Hrbek Mine, Svatá Dobrotivá (St. Benigna), Beroun, Bohemia, Czech Republic. National Museum Prague, PIN 18943 (sample NM). 8 × 5 cm. Photo L. Vrtiška.



Figure 5. Dark red beraunite crystal clusters with yellowish-brown hemispheres of cacoxenite. National Museum Prague, PIN 18943 (neotype specimen, sample NM). FOV 1 mm. Photo L. Vrtiška.

Optical measurements were performed on the original beraunite specimen (sample FR). Beraunite is optically biaxial (+), $\alpha = 1.768(2)$, $\beta = 1.781(3)$, $\gamma > 1.805$ (not exactly determined due to the lack of a suitable highly refractive liquid), $2V_{\text{meas}} = 69(4)^\circ$, and $2V_{\text{calc}}$ is not possible to calculate. Nevertheless, the direct measurement of α , β , and $2V$ angle allowed us to calculate the refractive index $\gamma_{\text{calc.}} = 1.809$. Dispersion of optical axes is strong, $r > v$. The orientation is $Y = b$, $X \approx a$, and $Z \approx c$. Pleochroism is strong; Z (brown red) $\gg Y > X$ (both brownish yellow).

4 Chemical composition

The chemical composition of beraunite was determined on polished and carbon-coated fragments mounted in an epoxy cylinder using a Cameca SX 100 electron microprobe

(Department of Mineralogy and Petrology, National Museum Prague). The instrument was operated in wavelength-dispersive mode at an accelerating voltage of 15 keV, beam current of 5 nA, and beam diameter of 7 μm . The following X-ray lines and standards were used: $K\alpha$ lines: P (apatite), Al (Al_2O_3), Fe (hematite), and Zn (ZnO). Other elements with $Z > 9$ were sought but not detected. Counting times were 10–20 s on peak and half of this time for each background position. The raw intensities were converted to the concentrations automatically using the procedure for improved quantitative microanalysis (PAP) (Pouchou and Pichoir, 1985) matrix-correction procedure. Water could not be analyzed directly because of the very small amount of material available; the H_2O presence was confirmed by Raman spectroscopy and its amount calculated by the stoichiometry of the ideal formula.

Analytical data for beraunite are given in Table 1. In the cationic position of the studied samples, Fe^{3+} dominates in the range from 5.45–5.69 apfu (sample NM) to 5.67–5.92 apfu (sample FR). In addition to iron, studied beraunites contain a small amount of Al (0.21–0.47 apfu in sample NM; 0.10–0.19 apfu in sample FR) and minor contents of Zn (up to 0.05 apfu in sample NM; up to 0.03 apfu in sample FR). Anion position contains only P.

The empirical formula of beraunite (FR) calculated on the basis of $\text{P} = 4$ apfu is $(\text{Fe}_{5.76}^{3+}\text{Al}_{0.15}\text{Zn}_{0.01})_{5.92}(\text{PO}_4)_{4.00}\text{O}_{0.99}(\text{OH})_{3.77} \cdot 6\text{H}_2\text{O}$.

The empirical formula of beraunite (NM) calculated on the basis of $\text{P} = 4$ apfu is $(\text{Fe}_{5.57}^{3+}\text{Al}_{0.31}\text{Zn}_{0.02})_{5.90}(\text{PO}_4)_{4.00}\text{O}_{0.99}(\text{OH})_{3.69} \cdot 6\text{H}_2\text{O}$.

The ideal formula of beraunite is $\text{Fe}_6^{3+}(\text{PO}_4)_4\text{O}(\text{OH})_4 \cdot 6\text{H}_2\text{O}$, which requires Fe_2O_3 52.82 %, P_2O_5 31.29 %, H_2O 15.89 %, and total 100 %.

5 Mössbauer spectroscopy

The transmission ^{57}Fe Mössbauer spectrum was collected at room temperature using a conventional Mössbauer spectrometer (MS2006 type based on virtual instrumentation technique; Pechoušek et al., 2012) in transmission geometry (constant acceleration mode) with a ^{57}Co (in Rh matrix) radioactive source (1.85 GBq) and fast scintillation detector with an $\text{YAlO}_3:\text{Ce}$ crystal. Carefully hand-picked crystals of beraunite were ground under isopropyl alcohol to avoid possible iron oxidation. The hyperfine parameters were calibrated against a rolled metallic iron ($\alpha\text{-Fe}$) foil at room temperature. The spectrum was fitted by Lorentz functions using the CONFIT2000 software (Žák and Jirásková, 2006). The experimental error is $\pm 0.02 \text{ mm s}^{-1}$ for the hyperfine parameters and $\pm 3 \%$ for the relative spectral areas.

The room temperature ^{57}Fe Mössbauer spectrum of neo-type NM beraunite from type locality Hrbek (Fig. 6) was fitted with three Lorentzian doublets. The isomer shifts for all three doublets close to or below 0.5 mm s^{-1} (Table 2) imply that all iron atoms in beraunite structure are exclusively in

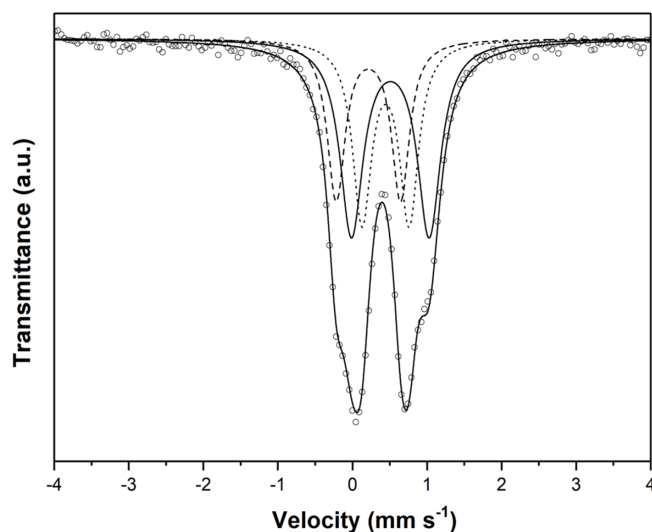


Figure 6. Mössbauer spectrum of beraunite from Hrbek (sample NM).

the form of Fe^{3+} , located at the M site with different next-nearest-neighbor configurations. There is no spectral evidence for Fe^{2+} or iron in some impurities (e.g., limonite). The spectrum, as well as derived hyperfine spectral parameters, is identical to eleonorite of Chukanov et al. (2017). Iron exclusively in trivalent form has already been stated in the original description of beraunite by Breithaupt (1840, 1841), and subsequently by Bořický (1867).

6 Raman spectroscopy

The Raman spectra of studied samples were collected in the range of $3600\text{--}50 \text{ cm}^{-1}$ using a DXR dispersive Raman spectrometer (Thermo Scientific) mounted on a confocal Olympus microscope. The Raman signal was excited by an unpolarized 633 nm He–Ne gas laser and detected by a CCD detector (size $1650 \times 200 \text{ mm}$, Peltier cooled to $-60 \text{ }^\circ\text{C}$, quantum efficiency 50 %, and dynamic range 360–1100 nm). The experimental parameters were $10\times$ objective, 2 s exposure time, 950 exposures, $50 \mu\text{m}$ pinhole spectrograph aperture, and 8 mW laser power level (estimated resolution $5.3\text{--}8.8 \text{ cm}^{-1}$, estimated spot size $1.3 \mu\text{m}$). The spectra were repeatedly acquired from different grains in order to obtain a representative spectrum with the best signal-to-noise ratio. The possible thermal damage of the measured point was excluded by visual inspection of the exposed surface after measurement, by observation of possible decay of spectral features at the start of excitation, and by checking for thermal downshift of Raman lines. The instrument was set up by a software-controlled calibration procedure using multiple neon emission lines (wavelength calibration), multiple polystyrene Raman bands (laser-frequency calibration), and standardized white-light sources (intensity calibration).

Table 1. Chemical composition of beraunite from Hrbek.

	Mean	Sample NM						Mean	Sample FR					
		1	2	3	4	5	6		1	2	3	4	5	6
Fe ₂ O ₃	50.40	50.19	50.76	49.73	51.28	51.19	49.24	51.95	52.03	51.18	52.95	51.91	52.05	51.55
Al ₂ O ₃	1.77	1.60	1.60	2.13	1.37	1.21	2.69	0.85	0.91	1.09	0.55	0.77	1.01	0.78
ZnO	0.21	0.29	0.42	0.14	0.09	0.09	0.23	0.12	0.17	0.20	0.06	0.00	0.00	0.27
P ₂ O ₅	32.18	32.18	32.06	32.25	32.05	32.36	32.15	32.06	32.18	32.10	31.79	32.10	32.07	32.09
H ₂ O*	16.02	15.89	16.13	15.96	16.08	15.94	16.13	16.04	16.11	15.93	16.21	15.94	16.12	15.91
Total	100.57	100.15	100.97	100.21	100.87	100.79	100.44	101.00	101.40	100.50	101.56	100.72	101.25	100.60
Fe ³⁺	5.569	5.545	5.629	5.483	5.689	5.624	5.445	5.762	5.749	5.669	5.922	5.750	5.771	5.712
Al	0.306	0.277	0.278	0.368	0.238	0.208	0.466	0.148	0.157	0.189	0.096	0.134	0.175	0.135
Zn	0.023	0.031	0.046	0.015	0.010	0.010	0.025	0.013	0.018	0.022	0.007	0.000	0.000	0.029
ΣM	5.898	5.854	5.953	5.865	5.937	5.842	5.936	5.922	5.924	5.880	6.025	5.883	5.946	5.876
P	4.000	4.000	4.000	4.000	4.000	4.000	4.000	4.000	4.000	4.000	4.000	4.000	4.000	4.000
OH	3.693	3.561	3.859	3.596	3.810	3.527	3.809	3.767	3.773	3.639	4.075	3.650	3.838	3.629
H ₂ O	6.000	6.000	6.000	6.000	6.000	6.000	6.000	6.000	6.000	6.000	6.000	6.000	6.000	6.000

* H₂O could not be analyzed directly because of the minute amount of material available and was calculated on the basis of 6H₂O, from the ideal composition of beraunite-related minerals and on the basis of neutral charge balance (OH). Coefficients of the empirical formula were calculated on the basis of P = 4 apfu.

Table 2. Parameters of the Mössbauer spectrum of beraunite (NM sample).

	Doublet	Isomer shift (mm s ⁻¹)	Quadrupole splitting (mm s ⁻¹)	Line width (mm s ⁻¹)	Relative area (%)
1		0.51	1.04	0.36	42
2		0.21	0.86	0.28	26
3		0.44	0.63	0.29	32

Spectral manipulations were performed using the Omnic 9 software (Thermo Scientific).

The experimental Raman spectra of beraunite from both samples from the Hrbek mine are close to each other (Fig. 7); small differences are probably caused by the different orientations of studied grains. Raman bands at 3554 and 3517 (3554 and 3525 FR) cm⁻¹ are assigned to the ν OH stretching vibrations, and a broad band with a maximum at 3311 (3334 FR) cm⁻¹ is connected with vibrations of structurally distinct and differently strong hydrogen-bonded water molecules. The weak broad band at 1621 (1628 FR) cm⁻¹ is related to the ν₂ (δ) bending vibrations of water molecules. Bands at 1162, 1131, and 1067 (1157, 1137, and 1063 FR) cm⁻¹ are attributed to the ν₃ (PO₄)³⁻ triply degenerated antisymmetric stretching vibrations and that at 1013, 996, and 933 (1025, 991, and 937 FR) cm⁻¹ to the ν₁ (PO₄)³⁻ symmetric stretching vibrations. The band at 690 (676 FR) cm⁻¹ is assigned to the Fe³⁺...O–H bending vibration. The ν₄ (δ) (PO₄)³⁻ bending vibrations are connected with the bands at 607 and 571 (602, 569 FR) cm⁻¹ and the ν₂ (δ) (PO₄)³⁻ bending vibrations with the bands at 456 and 406 (462, 436, 399 FR) cm⁻¹. According to Frost et al. (2014), bands in the region 390–280 cm⁻¹ (382, 344, 297 NM; 371, 300 FR) may be related to the metal-oxygen stretching vibrations. The bands observed below 250 cm⁻¹

(242, 205, 155, 129, 102 NM; 242, 200, 154, 95 FR) may be described as external or lattice vibrations.

7 Infrared spectroscopy

An infrared spectrum of the beraunite neotype sample (Fig. 8a) was recorded by the attenuated total reflection (ATR) method with a diamond cell on a Nicolet iS5 spectrometer. Spectra over the 4000–390 cm⁻¹ range were obtained by the co-addition of 32 scans with a resolution of 4 cm⁻¹ and a mirror velocity of 0.4747 cm s⁻¹. Spectra were co-added to improve the signal-to-noise ratio.

In order to obtain IR absorption spectra of other samples of beraunite-group minerals used for comparison (Figs. 8b, c and 9), their powders were mixed with anhydrous KBr, pelletized, and analyzed using an ALPHA FTIR spectrometer (Bruker Optics) in the wavenumber range from 360 to 3800 cm⁻¹, at a resolution of 4 cm⁻¹. A total of 16 scans were collected for each spectrum. The IR spectrum of an analogous pellet of pure KBr was used as a reference. The assignment of absorption bands was made in accordance with Chukanov et al. (2017) and Aksenov et al. (2018).

Bands in the ranges of 2900–3600 and 1620–1630 cm⁻¹ correspond to O–H stretching vibrations of H₂O molecules and OH⁻ groups and to H–O–H bending vibrations of H₂O,

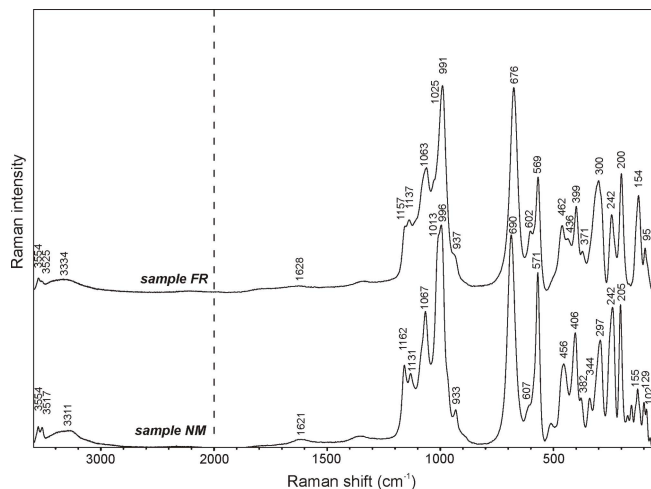


Figure 7. Raman spectra for beraunite from Hrbek (split at 2000 cm^{-1}); spectra are vertically shifted for comparison.

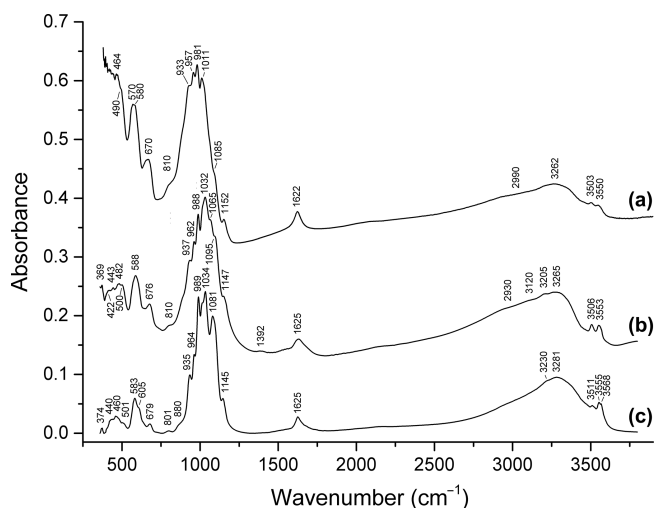


Figure 8. Infrared spectra of (a) beraunite neotype, (b) beraunite ($\text{Fe}_{5.76}\text{Al}_{0.18}\text{Mn}_{0.09}\text{Σ}6.03(\text{PO}_4)_{3.92}\text{O}(\text{OH})_{4.34} \cdot 5.98\text{H}_2\text{O}$) from the Rotläufchen mine (Chukanov et al., 2017), and (c) Mn-rich beraunite ($\text{Mn}_{0.58}^{2+}\text{Zn}_{0.13}\text{Mg}_{0.04}\text{Fe}_{5.24}^{3+}\text{Σ}5.98(\text{PO}_4)_4(\text{H}_2\text{O}, \text{OH}, \text{O})_{11}$) from Waidhaus, Upper Palatinate, Bavaria, Germany (Aksenov et al., 2018).

respectively. Bands in the ranges of $980\text{--}1160$, $930\text{--}970$, $570\text{--}680$ (partly), and $420\text{--}500$ (partly) cm^{-1} are assigned to $\nu_3(\text{F}_2)$ asymmetric stretching, $\nu_1(\text{A}_1)$ symmetric P–O stretching, $\nu_4(\text{F}_2)$ O–P–O bending, and $\nu_2(\text{E})$ O–P–O bending vibrations of PO_4^{3-} anions, respectively. Strictly speaking, bands in the ranges of $400\text{--}450$, $450\text{--}500$, and $480\text{--}600\text{ cm}^{-1}$ are resonance modes also involving $\text{V}^I\text{Fe}^{3+}\text{--O}$ - and $\text{V}^I\text{Al}\text{--O}$ -stretching vibrations (Chukanov and Chervonnyi, 2016). As a result, the substitution of divalent cations with trivalent ones results in high-frequency shifts of most bands in these ranges.

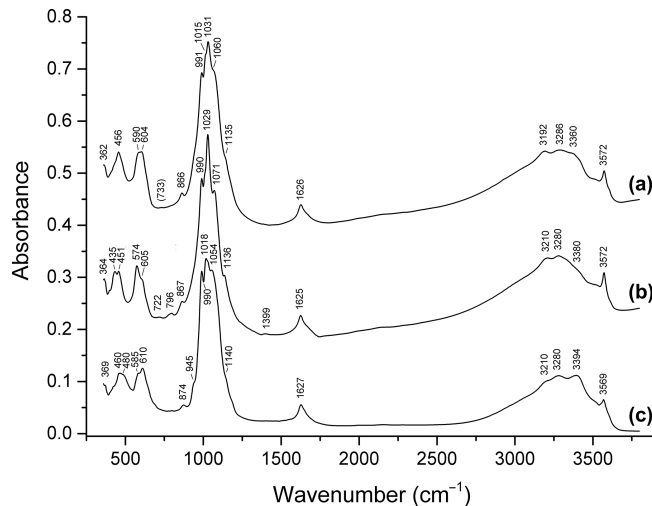


Figure 9. Infrared spectra of (a) dark blue ferroberaunite $\text{Fe}_{5.26}\text{Al}_{0.74}(\text{PO}_4)_{4.00}(\text{OH})_5 \cdot 6\text{H}_2\text{O}$ from Leveäniemi, Sweden; (b) green fibrous zincoberaunite $\text{Zn}_{0.92}\text{Fe}_{4.71}\text{Al}_{0.21}\text{Cr}_{0.10}(\text{PO}_4)_{4.00}(\text{OH})_5 \cdot 6\text{H}_2\text{O}$ from Hagendorf, Bavaria, Germany; and (c) intermediate member of the tvrdýite–beraunite series $\text{Ca}_{0.05\text{--}0.08}\text{Zn}_{0.34\text{--}0.50}\text{Mn}_{0.04\text{--}0.97}\text{Mg}_{0\text{--}0.05}\text{Fe}_{3.85\text{--}3.99}\text{Al}_{1.44\text{--}1.66}\text{Cr}_{0.06}(\text{PO}_4)_{4.00}(\text{OH})_5 \cdot 6\text{H}_2\text{O}$ from Hagendorf.

In the IR spectra of all beraunite-group minerals containing divalent cations, bands in the range of $3560\text{--}3572\text{ cm}^{-1}$ are observed. These bands are assigned to OH^- groups coordinating Fe^{2+} , Mn^{2+} , and/or Zn^{2+} . Corresponding $\text{M}^{2+}\dots\text{O}\text{--H}$ bending bands are observed in the range of $670\text{--}880\text{ cm}^{-1}$. Bands in the ranges of $3560\text{--}3572$ and $860\text{--}880$ are absent in the IR spectra of beraunite samples that do not contain admixed bivalent cations. Bands in the range of $670\text{--}680\text{ cm}^{-1}$ are absent in bivalent cation members and are present in samples without bivalent cations. In the IR spectra of Mn^{2+} -rich beraunite in which the M1 site has a mixed occupancy ($\text{Fe}^{3+} + \text{Mn}^{2+}$), a doublet $3555 + 3568\text{ cm}^{-1}$ is observed (Fig. 8c). The bands in the ranges of $800\text{--}810$ and $3500\text{--}3555\text{ cm}^{-1}$ are due to $\text{Fe}^{3+}\dots\text{O}\text{--H}$ bending and stretching vibrations involving OH^- groups coordinating with Fe^{3+} .

A specific feature of beraunite is the presence of very weak absorptions at ~ 1390 and $2930\text{--}2990\text{ cm}^{-1}$, which may be due to vibrations of P–OH and H^+ (Chukanov, 2014). The presence of trace amounts of HPO_4^{2-} and dynamic equilibrium $\text{HPO}_4^{2-} \leftrightarrow \text{PO}_4^{3-} + \text{H}^+$ are typical for hydrous phosphates. This assumption is in agreement with a minor deficit of cations in the empirical formula of the original beraunite sample.

Table 3. X-ray powder patterns of beraunite from Hrbek (samples NM and FR) compared with data for eleonorite from the Rotläufchen mine.

Hrbek (sample NM)			Hrbek (sample FR)						Rotläufchen mine	
$I_{\text{obs.}}$	$d_{\text{obs.}}$	$d_{\text{calc.}}$	$I_{\text{obs.}}$	$d_{\text{obs.}}$	$d_{\text{calc.}}$	h	k	l	$I_{\text{obs.}}$	$d_{\text{obs.}}$
100.0	10.3113	10.2938	100.0	10.3085	10.3065	2	0	0	100	10.41
19.3	9.6105	9.5934	14.3	9.6085	9.6018	0	0	2	38	9.67
11.4	7.2559	7.2473	8.3	7.2571	7.2537	2	0	-2	29	7.30
0.3	6.8150	6.8094				2	0	2	1	6.84
4.6	5.1500	5.1469	4.1	5.1524	5.1533	4	0	0	4	5.162
9.5	4.8125	4.8110	8.2	4.8125	4.8123	1	1	1	31	4.816
0.6	4.6640	4.6581				4	0	-2		
2.5	4.4575	4.4556	2.5	4.4571	4.4592	2	0	-4	13	4.424
3.3	4.4009	4.3993	3.1	4.4024	4.4010	1	1	2		
0.8	4.1159	4.1153	0.8	4.1146	4.1175	3	1	0	5	4.085
0.8	4.0546	4.0550	1.0	4.0525	4.0571	3	1	-1	4	4.051
2.2	3.7328	3.7318	1.2	3.7339	3.7342	3	1	2	9	3.737
0.8	3.6263	3.6237				4	0	-4	1	3.630
0.4	3.5220	3.5212	0.4	3.5219	3.5231	3	1	-3		
3.3	3.4854	3.4843	2.1	3.4842	3.4861	1	1	-4	13	3.481
15.4	3.4333	3.4313	14.0	3.4358	3.4355	6	0	0	18	3.432
2.9	3.4040	3.4033	2.8	3.4051	3.4058	3	1	3		
3.5	3.2989	3.2967	2.8	3.3008	3.3004	6	0	-2	3	3.304
1.2	3.2142	3.2142	0.9	3.2172	3.2168	5	1	0		
10.3	3.1986	3.1978	3.2	3.1998	3.2006	0	0	6	18	3.197
2.1	3.1712	3.1687	2.4	3.1743	3.1728	6	0	2		
1.4	3.1423	3.1451	3.2	3.1481	3.1478	5	1	1	11	3.153
3.5	3.1102	3.1093	1.7	3.1121	3.1118	2	0	-6		
10.0	3.0672	3.0671	6.6	3.0699	3.0695	3	1	4	34	3.071
1.0	2.8781	2.8770	0.4	2.8792	2.8798	6	0	-4	3	2.872
0.8	2.8610	2.8605				3	1	-5		
0.8	2.8171	2.8174	0.4	2.8187	2.8200	5	1	3	3	2.821
0.5	2.7956	2.7956				4	0	-6		
1.7	2.7326	2.7324	2.2	2.7351	2.7343	5	1	-4	10	2.722
3.2	2.7114	2.7110	2.1	2.7117	2.7127	1	1	-6		
0.3	2.6122	2.6120				5	1	4	1	2.614
6.2	2.5732	2.5734	2.7	2.5774	2.5766	8	0	0	9	2.574
			4.3	2.5722	2.5717	0	2	0		
0.8	2.5522	2.5530	0.7	2.5551	2.5555	7	1	0		
1.2	2.5263	2.5253	0.6	2.5282	2.5271	5	1	-5	1	2.525
0.7	2.4844	2.4836				0	2	2	2	2.483
0.4	2.4781	2.4786				2	2	-1		
0.7	2.4163	2.4166				7	1	-3	3	2.416
0.9	2.4063	2.4055				2	2	2		
0.9	2.3300	2.3281				7	1	3	2	2.331
0.2	2.3225	2.3243				5	1	-6		
0.9	2.3057	2.3061	0.7	2.3077	2.3080	7	1	-4	5	2.306
0.6	2.3005	2.3002	0.5	2.3013	2.3010	4	2	0	1	2.251
0.7	2.2280	2.2278	0.8	2.2296	2.2296	4	0	-8	2	2.227
0.5	2.2227	2.2228	0.3	2.2243	2.2238	4	2	2		
2.4	2.1070	2.1067	0.7	2.1075	2.1082	3	1	-8	6	2.105
1.0	2.0951	2.0970				4	2	-4		
0.3	2.0675	2.0668				9	1	-2	4	2.063
2.6	2.0589	2.0588	1.3	2.0611	2.0613	10	0	0	2	2.048
0.6	2.0383	2.0372				5	1	7	2	2.036
0.6	2.0036	2.0039	0.4	2.0048	2.0047	0	2	6	6	2.000
0.8	1.9958	1.9966	0.6	1.9978	1.9978	6	2	2		
0.3	1.9687	1.9687				5	1	-8	2	1.967
0.7	1.9195	1.9226	0.2	1.9247	1.9239	3	1	-9	6	1.919

Table 3. Continued.

Hrbek (sample NM)			Hrbek (sample FR)			Rotläufchen mine				
$I_{\text{obs.}}$	$d_{\text{obs.}}$	$d_{\text{calc.}}$	$I_{\text{obs.}}$	$d_{\text{obs.}}$	$d_{\text{calc.}}$	h	k	l	$I_{\text{obs.}}$	$d_{\text{obs.}}$
1.7	1.9182	1.9172	1.6	1.9186	1.9182	6	2	−4		
0.4	1.8785	1.8788	0.3	1.8807	1.8807	5	1	8	2	1.885
0.2	1.8770	1.8773				9	1	4		
0.7	1.8647	1.8647	0.5	1.8660	1.8663	3	1	9	2	1.864
0.6	1.7821	1.7818				1	1	10	1	1.780
0.7	1.7424	1.7422	0.4	1.7431	1.7430	2	2	−8	1	1.746
0.9	1.7210	1.7210				6	0	−10	2	1.719
0.6	1.7136	1.7156	0.5	1.7175	1.7178	12	0	0	2	1.708
0.5	1.7013	1.7017	0.6	1.7025	1.7029	6	2	6		
0.8	1.6834	1.6839				10	0	6	2	1.686
0.8	1.6834	1.6835				11	1	−4		
0.2	1.6813	1.6818				7	1	−9		
0.8	1.6714	1.6709				12	0	2		
0.5	1.6490	1.6484				12	0	−4	1	1.656
1.3	1.6070	1.6071				10	2	0	6	1.614
1.5	1.5991	1.5989				0	0	12	2	1.602
0.7	1.5338	1.5336				6	2	8	5	1.537
0.9	1.5327	1.5321				2	2	−10	1	1.520
0.4	1.4939	1.4942	0.8	1.4962	1.4959	8	0	10	2	1.498

Rotläufchen mine¹ – data published by Chukanov et al. (2017) for dark red beraunite (eleonorite); they also observed diffraction lines 3.976/1, 2.146/1, 1.976/2, 1.821/1, 1.793/2, 1.579/1, 1.569/2 plus 10 lines below 1.480 Å.

8 X-ray powder diffraction

Powder X-ray diffraction data for both beraunite samples (FR, NM) were collected on a Bruker D8 Advance diffractometer (National Museum, Prague) with a solid-state 1D LynxEye detector (width 2.05°) using $\text{CuK}\alpha$ radiation and operating at 40 kV and 40 mA. For minimizing the background of the scan, the powder sample was placed onto the surface of a flat silicon wafer from acetone suspension. The powder pattern was collected using Bragg–Brentano geometry in the range 3–70° 2θ , in 0.01° steps with a counting time of 8 s per step. Positions and intensities of reflections were found and refined using the Pearson VII profile-shape function with the ZDS program package (Ondruš, 1993), and the unit-cell parameters were refined by the least-squares algorithm implemented by Burnham (1962). The experimental powder pattern was indexed in line with the calculated values of intensities obtained by the PowderCell 2.3 program (Kraus and Nolze, 1996) from the results of our crystal structure study of beraunite (see below).

The experimental patterns of both samples (Table 3) are comparable and agree very well with the X-ray pattern calculated from the results of our single-crystal study and published data for eleonorite from Rotläufchen mine (Chukanov et al., 2017). Experimental intensities are partly affected by the preferred orientation as well as by the small amount of material available for the study (especially in the case of the FR sample). The refined unit-cell parameters are compared in Table 4 with the published data.

9 Single-crystal X-ray diffraction

For the single-crystal diffraction experiment, a short-prismatic brownish-red single crystal was separated from the fragment of the original beraunite specimen (FR), examined under a polarizing microscope and mounted on a glass fiber. The diffraction experiment (see Table 5 for details) was performed at room temperature with a Rigaku SuperNova single-crystal diffractometer equipped with the Atlas S2 CCD detector and a microfocus $\text{MoK}\alpha$ source. Data reduction was performed using CrysAlisPro Version 1.171.39.46 (Rigaku, 2019). The data were corrected for the Lorentz factor and polarization effect. Absorption correction (empirical scaling using spherical harmonics) was applied in Jana2006 (Petříček et al., 2014). A single-crystal X-ray experiment revealed a monoclinic unit cell (Table 5).

Initially, the structure of beraunite was solved from the X-ray data using the intrinsic phasing algorithm of the SHELXT program (Sheldrick, 2015) in the $C2/c$ space group, as was indicated by the space-group test ($R_{\text{int}} = 0.0331$ for 2222 reflections with $I > 3\sigma(I)$ from averaging). The subsequent refinement using the full-matrix least-squares algorithm of the Jana2006 program revealed the same general model as has been provided for the beraunite-related structures (Fanfani and Zanazzi, 1969; Moore and Kampf, 1992; Chukanov et al., 2017; Aksenov et al., 2018; Tvrdý et al., 2020). With the complete model in the $C2/c$ space group, including anisotropic atomic displacement parameters for all atoms and apparently visible po-

Table 4. Unit-cell parameters for beraunite.

				<i>a</i> [Å]	<i>b</i> [Å]	<i>c</i> [Å]	β [°]	<i>V</i> [Å ³]
Hrbek	FR	<i>S</i> ¹	[1]	20.6507(6)	5.1377(2)	19.2152(5)	93.523(2)	2034.82(11)
Hrbek	FR	<i>P</i> ²	[1]	20.653(2)	5.1433(6)	19.241(2)	93.560(9)	2039.9(2)
Hrbek	NM	<i>P</i> ²	[1]	20.627(2)	5.1426(8)	19.224(2)	93.578(11)	2035.3(4)
Rotläufchen		<i>S</i> ¹	[2]	20.679(10)	5.148(2)	19.223(9)	93.574(9)	2042.5(16)
Rotläufchen		<i>P</i> ²	[2]	20.694(6)	5.143(1)	19.236(7)	93.52(2)	2044(2)

¹ – single-crystal X-ray diffraction data; ² – powder X-ray diffraction data; [1] this proposal; [2] Chukanov et al. (2017).

Table 5. Details for the data collection and refinement of the structure of beraunite.

Crystal data	
Chemical formula	Fe ₆ H ₁₆ O ₂₇ P ₄
<i>M_r</i>	907.1
Crystal system, space group	Monoclinic, <i>Cc</i>
Temperature (K)	298
<i>a</i> , <i>b</i> , <i>c</i> (Å)	20.6507(6), 5.1377(2), 19.2152(5)
β (°)	93.523(2)
<i>V</i> (Å ³)	2034.82(11)
<i>Z</i>	4
Radiation type	Mo <i>K</i> α
μ (mm ⁻¹)	4.61
Crystal size (mm)	0.04 × 0.04 × 0.01
Data collection	
Diffractometer	Rigaku SuperNova CCD
Absorption correction	Empirical (using intensity measurements) Jana2006
<i>T</i> _{min} , <i>T</i> _{max}	0.891, 1.000
No. of measured, independent, and observed [<i>I</i> > 3 σ (<i>I</i>)] reflections	15639, 4951, 4239
<i>R</i> _{int}	0.031
(<i>sin</i> θ / λ) _{max} (Å ⁻¹)	0.696
Refinement	
<i>R</i> [<i>F</i> ² > 3 σ (<i>F</i> ²)], <i>wR</i> (<i>F</i> ²), <i>S</i>	0.027, 0.062, 1.04
No. of reflections	4951
No. of parameters	383
No. of restraints	20
H-atom treatment	All H-atom parameters refined
$\Delta\rho_{\text{max}}$, $\Delta\rho_{\text{min}}$ (<i>e</i> Å ⁻³)	0.50, -0.58
Absolute structure	2350 of Friedel pairs used in the refinement
Absolute structure parameter	0.05(2)

sitions of the H atoms in the difference Fourier maps, it was not possible to reach significantly reasonable indices of agreement ($R_{\text{obs}} = 0.0788$, $wR_{\text{obs}} = 0.2186$; $R_{\text{all}} = 0.0906$, $wR_{\text{all}} = 0.2222$, $\text{GOF}_{\text{obs}} = 2.70$, $\text{GOF}_{\text{all}} = 2.55$; 2220 observed $I > 3\sigma(I)$, and 2549 all unique reflections). Such suspiciously high *R* values and namely the goodness-of-fit value, along with the higher values of the difference Fourier electron density (largest peak of $1.71 e \text{ \AA}^{-3}$) and its distribution (namely “doubled” symmetrical peaks nearby O atoms which should belong, otherwise, to OH groups, thus partially occupied H sites at best), made us convinced that the real

beraunite structure belongs to the lower-syngony group. The attempt of the refinement in the non-centrosymmetric space group *Cc* (treated in the refinement as twinned by merohedry – inversion twin; Petříček et al., 2016) led to a tremendous improvement of the fit; the drop was about 4%. The final refinement, including all H atoms flawlessly located from the difference Fourier maps, smoothly converged to the final $R_{\text{obs}} = 0.0270$ for 4239 unique reflections of $I > 3\sigma(I)$ with a $\text{GOF}_{\text{obs}} = 1.14$; the highest peak that resides in the electron density was $0.50 e \text{ \AA}^{-3}$, only. The details for the refinement are given in Table 5. Atom coordinates, atomic displacement

Table 6. Atom coordinates and displacement parameters (as isotropic or equivalent; Å²) for the structure of beraunite.

Atom	<i>x/a</i>	<i>y/b</i>	<i>z/c</i>	<i>U</i> _{iso} [*] / <i>U</i> _{eq}
Fe1 (<i>M1</i>)	0.50074(11)	0.01427(19)	0.49595(10)	0.00731(16)
Fe2_1 (<i>M4_1</i>)	0.60628(10)	1.03671(16)	0.41018(9)	0.0085(2)
Fe2_2 (<i>M4_2</i>)	-0.60762	-1.02150	-0.41345	0.0062(2)
Fe3_1 (<i>M3_1</i>)	0.45976(10)	0.27275(16)	0.32992(9)	0.0071(2)
Fe3_2 (<i>M3_2</i>)	-0.45263	-0.26043	-0.32508	0.0072(2)
Fe4 (<i>M2</i>)	0.74997(11)	0.7646(2)	0.49850(10)	0.00877(16)
P1_1	0.39636(12)	0.4926(3)	0.47330(11)	0.0050(4)
P1_2	-0.39479	-0.4653	-0.47326	0.0051(4)
P2_1	0.59394(12)	0.5475(3)	0.31658(11)	0.0074(4)
P2_2	-0.59073	-0.5264	-0.31860	0.0061(4)
O1	0.5043(3)	0.0973(5)	0.2527(3)	0.0104(8)
O2_1	0.5221(2)	0.5573(8)	0.3268(2)	0.0101(11)
O2_2	-0.5183	-0.5293	-0.3349	0.0115(12)
O3_1	0.4282(2)	0.2639(8)	0.5164(2)	0.0076(11)
O3_2	-0.4286	-0.2487	-0.5185	0.0088(11)
O4_1	0.3241(2)	0.5029(8)	0.4838(2)	0.0084(11)
O4_2	-0.3226	-0.4728	-0.4868	0.0077(11)
O5_1	0.5099(2)	0.0751(8)	0.3994(2)	0.0096(11)
O5_2	-0.5051	-0.0215	-0.3964	0.0077(10)
O6_1	0.6299(2)	0.3498(8)	0.3641(2)	0.0101(11)
O6_2	-0.6294	-0.3319	-0.3656	0.0109(11)
O7_1	0.6232(2)	0.8151(8)	0.3336(2)	0.0093(12)
O7_2	-0.6188	-0.7988	-0.3347	0.0109(12)
O8_1	0.4263(2)	0.7521(7)	0.5019(2)	0.0071(11)
O8_2	-0.4233	-0.7311	-0.4937	0.0119(12)
O9_1	0.6905(2)	1.0285(8)	0.4613(2)	0.0094(12)
O9_2	-0.6908	-1.0065	-0.4635	0.0100(12)
O10_1	0.6050(2)	0.4840(8)	0.2398(2)	0.0121(12)
O10_2	-0.5998	-0.4623	-0.2427	0.0109(12)
O11_1	0.7466(2)	0.9248(9)	0.5977(2)	0.0162(13)
O11_2	-0.7467	-0.9071	-0.5982	0.0138(13)
O12_1	0.4094(2)	0.4661(8)	0.3969(2)	0.0107(11)
O12_2	-0.4034	-0.4110	-0.3974	0.0154(12)
O13_1	0.3896(2)	-0.0275	0.3227(3)	0.0181(14)
O13_2	-0.3820	0.0342(9)	-0.3212	0.0184(14)
O14_1	0.7339(3)	0.6513(12)	0.7150(3)	0.0353(19)
O14_2	-0.7288	-0.6538	-0.7166	0.0331(18)
H1o11_1	0.7891(11)	0.986(8)	0.612(3)	0.0195*
H1o11_2	-0.774	-1.052	-0.610	0.0165*
H1o9_1	0.694(3)	1.171(7)	0.493(2)	0.0112*
H1o9_2	-0.696	-1.182	-0.478	0.012*
H2o11_2	-0.737	-0.833	-0.6417	0.0165*
H1o14_1	0.752(2)	0.497(7)	0.735(3)	0.0423*
H1o1	0.500(3)	-0.075	0.265(2)	0.0124*
H1o13_1	0.399(3)	-0.181	0.348(2)	0.0217*
H2o13_1	0.377(2)	-0.065	0.2756(10)	0.0217*
H1o5_2	-0.507	0.133(5)	-0.371	0.0092*
H2o14_1	0.6910(11)	0.657(10)	0.729(3)	0.0423*
H2o14_2	-0.7605	-0.523	-0.723	0.0397*
H1o13_2	-0.3494	0.052(11)	-0.353	0.0221*
H2o11_1	0.743(2)	0.758(5)	0.619(2)	0.0195*
H2o13_2	-0.393	0.203(5)	-0.307	0.0221*
H1o14_2	-0.6888	-0.565	-0.715	0.0397*

* Refined with the isotropic displacement parameter. *M* denotes the metal cation site labeling according to Moore and Kampf (1992), taking into account the independency (expressed as *M4_1* and *M4_2*) of the particular site due to symmetry lowering $C2/m \rightarrow Cc$ in beraunite.

Table 7. Selected interatomic distances (Å) and polyhedral measures for beraunite.

Fe1–O3_1	2.029(5)	Fe2_1–O3_2 ⁱⁱ	2.161(5)	Fe2_2–O3_1 ^{vi}	2.153(4)
Fe1–O3_2 ⁱⁱⁱ	2.021(5)	Fe2_1–O5_1 ^{iv}	1.997(5)	Fe2_2–O5_2 ⁱ	2.123(5)
Fe1–O5_1	1.902(5)	Fe2_1–O6_1 ^{iv}	1.913(4)	Fe2_2–O6_2 ⁱ	1.908(4)
Fe1–O5_2 ⁱⁱⁱ	2.087(5)	Fe2_1–O7_1	1.910(4)	Fe2_2–O7_2	1.923(5)
Fe1–O8_1 ⁱ	2.053(5)	Fe2_1–O8_2 ^v	2.312(5)	Fe2_2–O8_1 ^{vii}	2.150(5)
Fe1–O8_2 ⁱⁱ	2.042(5)	Fe2_1–O9_1	1.946(5)	Fe2_2–O9_2	1.918(5)
<Fe1–Φ >	2.022	<Fe2_1–Φ >	2.040	<Fe2_2–Φ >	2.029
$V_{\text{Fe1}\Phi}$	10.58 Å ³	$V_{\text{Fe2}_1\Phi}$	10.81 Å ³	$V_{\text{Fe2}_2\Phi}$	10.70 Å ³
ECoN _{Fe1Φ}	5.748	ECoN _{Fe2_1Φ}	4.970	ECoN _{Fe2_2Φ}	5.188
Distortion _{Fe1Φ}	8.165	Distortion _{Fe2_1Φ}	53.009	Distortion _{Fe2_2Φ}	31.188
Fe3_1–O1	2.007(5)	Fe3_2–O1 _{ix}	1.973(5)	Fe4–O4_1 ^x	1.994(5)
Fe3_1–O2_1	1.951(5)	Fe3_2–O2_2	1.937(5)	Fe4–O4_2 ⁱⁱ	1.966(5)
Fe3_1–O5_1	1.929(4)	Fe3_2–O5_2	2.092(4)	Fe4–O9_1	1.936(4)
Fe3_1–O10_2 ^{viii}	2.048(5)	Fe3_2–O10_1 ^{ix}	2.027(5)	Fe4–O9_2 ^{xi}	1.965(4)
Fe3_1–O12_1	1.973(5)	Fe3_2–O12_2	1.933(5)	Fe4–O11_1	2.081(5)
Fe3_1–O13_1	2.116(5)	Fe3_2–O13_2	2.100(5)	Fe4–O11_2 ^{xi}	2.062(5)
<Fe3_1–Φ >	2.004	<Fe3_2–Φ >	2.010	<Fe4–Φ >	2.000
$V_{\text{Fe3}_1\Phi}$	10.67 Å ³	$V_{\text{Fe3}_2\Phi}$	10.78 Å ³	$V_{\text{Fe4}\Phi}$	10.65 Å ³
ECoN _{Fe3_1Φ}	5.767	ECoN _{Fe3_2Φ}	5.723	ECoN _{Fe4Φ}	5.836
Distortion _{Fe3_1Φ}	9.912	Distortion _{Fe3_2Φ}	11.612	Distortion _{Fe4Φ}	7.048
P1_1–O3_1	1.559(5)	P1_2–O3_2	1.547(5)		
P1_1–O4_1	1.521(5)	P1_2–O4_2	1.529(5)		
P1_1–O8_1	1.557(5)	P1_2–O8_2	1.526(5)		
P1_1–O12_1	1.515(5)	P1_2–O12_2	1.503(5)		
<P1_1–Φ >	1.538	<P1_2–Φ >	1.526		
P2_1–O2_1	1.511(5)	P2_2–O2_2	1.547(6)		
P2_1–O6_1	1.527(5)	P2_2–O6_2	1.538(5)		
P2_1–O7_1	1.528(5)	P2_2–O7_2	1.538(5)		
P2_1–O10_1	1.542(5)	P2_2–O10_2	1.517(5)		
<P2_1–Φ >	1.527	<P2_2–Φ >	1.535		

Symmetry codes: ⁱ $x, y-1, z$; ⁱⁱ $x+1, y+1, z+1$; ⁱⁱⁱ $x+1, y, z+1$; ^{iv} $x, y+1, z$; ^v $x+1, y+2, z+1$; ^{vi} $x-1, y-1, z-1$; ^{vii} $x-1, y-2, z-1$; ^{viii} $x+1, -y, z+1/2$; ^{ix} $x-1, -y, z-1/2$; ^x $x+1/2, y+1/2, z$; ^{xi} $x+3/2, y+3/2, z+1$. ECoN – effective coordination number (Hoppe, 1979); distortion – octahedral distortion (Brown and Shannon, 1973).

parameters, and site occupancies are given in Table 6 (the atom names denoted as X_1 or X_2 , where X is the corresponding atom, refer to an original single site in the holoedry model), selected interatomic distances in Table 7, hydrogen-bond geometry in Table 8, and bond-valence analysis in Table 9.

10 Crystal structure

Beraunite possesses a well-known type of structure, which is widespread among the basic phosphates of ferrous and ferric iron (Moore, 1969, 1970). Characteristic fundamental building blocks are trimers of face-shared $M1$ and $M4$ octahedra, where the inner $[M1O_4(OH)_2]$ octahedron occupies the $4a$ site, and the outer $[M4O_4(OH)(OH)_2]$ octahedra occupy the $8f$ sites, for the $C2/c$ structures. The trimers are further linked via two isolated $[P1O_4]$ tetrahedra along the b direc-

tion, and along the c , they are connected by corner-sharing with $[M3O_3(OH)_2(H_2O)]$ octahedra and $[P2O_4]$ tetrahedra, which results in heteropolyhedral layers (Fig. 10). These layers are then linked via $M2$ octahedra, forming a framework containing wide channels running parallel to b and hosting H_2O . The seven octahedra structural blocks (triplets with corner-shared octahedra) are referred to as the h clusters by Moore (1969, 1970).

The above-given description and structure symmetry were considered valid for all beraunite-like minerals, including those containing all iron as trivalent (Chukanov et al., 2017; Aksenov et al., 2018).

For the currently investigated type specimen of beraunite, the symmetry of the structure was unambiguously found to be lower (Cc) than for the other members reported in the past ($C2/c$). It bears the following consequences. The $M1$ distorted octahedron was found to contain $Fe^{3+}O_4P O_h OH_h$ (where P denominates O linked to PO_4 , and h represents

Table 8. Hydrogen-bond geometry (Å, °) in the crystal of beraunite.

<i>D</i> –H... <i>A</i>	<i>D</i> –H (Å)	H... <i>A</i> (Å)	<i>D</i> ... <i>A</i> (Å)	<i>D</i> –H... <i>A</i> (°)
O11_1–H1o11_1...O6_2 ^{xi}	0.96(3)	1.95(3)	2.897(6)	170(4)
O11_2–H1o11_2...O6_1 ^{xiv}	0.95(4)	2.08(4)	2.890(6)	142(3)
O9_1–H1o9_1...O4_2 ^v	0.96(4)	1.90(4)	2.769(6)	149(4)
O9_2–H1o9_2...O4_1 ^{vii}	0.95(2)	1.83(3)	2.741(6)	159(5)
O11_2–H2o11_2...O14_2	0.95(3)	1.73(3)	2.667(7)	170(4)
O14_1–H1o14_1...O14_2 ^{xxi}	0.94(4)	2.02(4)	2.954(8)	169(4)
O1–H1o1...O2_1 ⁱ	0.92(2)	2.26(3)	3.129(5)	156(4)
O13_1–H1o13_1...O12_1 ⁱ	0.95(4)	2.04(3)	2.984(6)	172(4)
O13_1–H2o13_1...O7_2 ^{xxv}	0.94(2)	2.24(3)	3.147(7)	161(4)
O5_2–H1o5_2...O2_2 ^{iv}	0.93(3)	1.89(3)	2.812(6)	170(3)
O5_2–H1o5_2...O7_2 ^{iv}	0.93(3)	2.47(5)	2.928(6)	110(3)
O14_1–H2o14_1...O10_1 ^{xxvi}	0.94(3)	1.94(3)	2.818(7)	154(5)
O14_2–H2o14_2...O14_1 ^{xxvii}	0.94(4)	2.25(5)	2.977(8)	134(4)
O13_2–H1o13_2...O11_1 ^{vi}	0.94(4)	2.34(4)	3.211(7)	153(4)
O11_1–H2o11_1...O14_1	0.95(3)	1.95(4)	2.683(7)	132(3)
O13_2–H2o13_2...O10_1 ^{xxviii}	0.94(3)	1.84(3)	2.759(6)	164(5)
O14_2–H1o14_2...O10_2 ^{xxix}	0.94(3)	1.95(3)	2.806(7)	150(4)

Symmetry codes: ⁱ $x, y-1, z$; ^{iv} $x, y+1, z$; ^v $x+1, y+2, z+1$; ^{vi} $x-1, y-1, z-1$; ^{vii} $x-1, y-2, z-1$; ^{xi} $x+3/2, y+3/2, z+1$; ^{xiv} $x-3/2, y-3/2, z-1$; ^{xxi} $x+3/2, -y-1/2, z+3/2$; ^{xxv} $x+1, -y-1, z+1/2$; ^{xxvi} $x, -y+1, z+1/2$; ^{xxvii} $x-3/2, -y+1/2, z-3/2$; ^{xxviii} $x-1, -y+1, z-1/2$; ^{xxix} $x, -y-1, z-1/2$.

Table 9. Bond-valence analysis for the structure of beraunite (values in valence units, vu).

	Fe1	Fe2_1	Fe2_2	Fe3_1	Fe3_2	Fe4	P1_1	P1_2	P2_1	P2_2	\sum BV – H	\sum BV + H
O1				0.51	0.56						1.07	2.07
O2_1				0.60					1.33		1.93	1.98
O2_2					0.62					1.21	1.83	1.93
O3_1	0.48		0.34				1.18				2.00	2.00
O3_2	0.49	0.33						1.20			2.03	2.03
O4_1						0.53	1.30				1.83	1.95
O4_2						0.57		1.27			1.84	1.94
O5_1	0.69	0.53		0.64							1.85	1.85
O5_2	0.41		0.37		0.40						1.19	2.16
O6_1		0.66							1.27		1.94	2.00
O6_2			0.67							1.24	1.91	2.00
O7_1		0.67							1.27		1.94	1.94
O7_2			0.66							1.24	1.89	1.93
O8_1	0.45		0.34				1.19				1.98	1.98
O8_2	0.46	0.22						1.27			1.95	1.95
O9_1		0.61				0.62					1.23	2.14
O9_2			0.66			0.58					1.23	2.16
O10_1					0.48				1.23		1.72	1.92
O10_2			0.46							1.30	1.76	1.85
O11_1						0.42					0.42	2.29
O11_2						0.44					0.44	2.30
O12_1				0.56			1.32				1.88	1.95
O12_2					0.63			1.34			1.97	1.97
O13_1			0.38								0.38	2.23
O13_2					0.40						0.40	2.29
O14_1											0.00	2.03
O14_2											0.00	2.12
\sum BV	2.99	3.02	3.03	3.14	3.10	3.16	4.98	5.08	5.10	4.99		

Bond-valence parameters taken from Gagné and Hawthorne (2015).

Table 10. Comparative data for beraunite and related minerals.

Name actually valid	Beraunite ^a	Ferroberaunite ^b	Zincoberaunite	Tvrđýte
Previous name	Eleonorite	Beraunite		
Idealized formula	$\text{Fe}_6^{3+}(\text{PO}_4)_4\text{O}(\text{OH})_4 \cdot 6\text{H}_2\text{O}$	$\text{Fe}^{2+}\text{Fe}_5^{3+}(\text{PO}_4)_4(\text{OH})_5 \cdot 6\text{H}_2\text{O}$	$\text{ZnFe}_5^{3+}(\text{PO}_4)_4(\text{OH})_5 \cdot 6\text{H}_2\text{O}$	$\text{Fe}^{2+}\text{Fe}_2^{3+}\text{Al}_3(\text{PO}_4)_4(\text{OH})_5 \cdot 6\text{H}_2\text{O}$
Site <i>M1</i>	Fe^{3+}	Fe^{2+}	Zn	Fe^{2+}
Site <i>M4</i>	Fe^{3+}	Fe^{3+}	Fe^{3+}	Fe^{3+}
Sites <i>M2+M3</i>	Fe^{3+}	Fe^{3+}	Fe^{3+}	Al
Crystal system	Monoclinic	Monoclinic	Monoclinic	Monoclinic
Space group	<i>Cc</i>	<i>C2/c</i>	<i>C2/c</i>	<i>C2/c</i>
<i>a</i> (Å)	20.6507(6)	20.8708(3)	20.837(2)	20.564(4)
<i>b</i> (Å)	5.1377(2)	5.1590(8)	5.1624(4)	5.1010(10)
<i>c</i> (Å)	19.2152(5)	19.2263(3)	19.250(1)	18.883(4)
β (°)	93.523(2)	93.3186(17)	93.252(5)	93.68(3)
Volume (Å ³)	2034.82(11)	2066.7(3)	2067.3(3)	1976.7(7)
<i>Z</i>	4	4	4	4
Optical	Biaxial (+)	Biaxial (–)	Biaxial (–)	Biaxial (–)
α	1.768	1.736	1.745	1.650
β	1.781	1.765	1.760	1.671
γ	>1.805	1.786	1.770	1.677
2 <i>V</i>	69° (meas.)	68° (meas.)/71° (calc.)	80°	56°
Density	2.961 (calc.)	2.907 (calc.)	2.938 (calc.)	2.834 (calc.)
References	this paper	Tvrđý et al. (2022)	Chukanov et al. (2016)	Sejkora et al. (2016)

^a Beraunite – defined on the basis of the present study of the original beraunite specimen sample; at the same time, eleonorite is discredited. ^b Ferroberaunite – new name for mixed-valence iron member (Tvrđý et al., 2021).

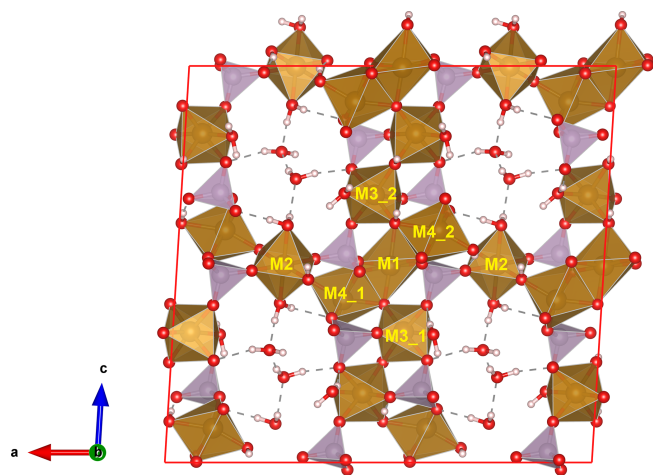


Figure 10. Crystal structure of beraunite viewed perpendicular to the crystal elongation. The heteropolyhedral slabs are connected by the *M2* octahedra; water molecules located in channels are hydrogen bonded (dashed lines). P tetrahedra are purple, O atoms red, and H atoms grey. The unit cell is outlined.

O atoms of the further linkage within the trimer). Those (O_hOH_h) represented by a single atom in *C2/c* (see, for instance, OH1 of Aksenov et al., 2018; or O_2 of Tvrđý et al., 2020) are now represented by two independent atoms in *Cc* and labeled as O5_1 and O5_2 . Bond-valence calculations clearly indicated (Table 9) that the O5_1 site has a value of 1.869(17) vu acceptable for O^{2-} , while the O5_2 site has a considerably lower bond valence of 1.214(9) vu. Thus, the value is characteristic for the OH group (Brown,

2002). This finding is in line with the fact that all sites in beraunite studied are occupied by the ferric iron, and the demand for electroneutrality then requires the presence of one deprotonated O atom and one OH group within the *M1* octahedron (Fig. 11) instead of two OH groups. This leads to an overall composition of the structural unit in beraunite given as $\{\text{Fe}_6(\text{PO}_4)_4\text{O}(\text{OH})_4\}^0$. The desymmetrization of the structure is governed by the occupancy of the octahedral *M* sites (all Fe is trivalent) and a consequent change of the H-bonding system (transferring the electro-valence charges within the structure).

11 Discussion

In view of recent conclusions on the structure of beraunite obtained from the type specimen, the status of the mineral eleonorite, $\text{Fe}_6^{3+}(\text{PO}_4)_4\text{O}(\text{OH})_4 \cdot 6\text{H}_2\text{O}$ (Chukanov et al., 2017), has been now questioned again. Eleonorite has been known for a long-time (Nies, 1877, 1880; Streng, 1881; Palache et al., 1951), but, as Chukanov et al. (2017) also stressed it has always had an ambiguous status. Chukanov et al. (2017) stated that already at that time it was “considered to be an oxidized variety of beraunite”. We have to re-emphasize that beraunite was already described by Breithaupt in 1840 (Breithaupt, 1840), therefore more than 30 years before eleonorite. According to Breithaupt (1840, 1841), beraunite from the type discovery is “dunkel hyacinthroth” (dark hyacinth red) in color and when exposed to the sun transforms to reddish brown. Eleonorite in crystals is, according to Chukanov et al. (2017), red-brown. Chukanov et al. (2017) do not provide any reference for their state-

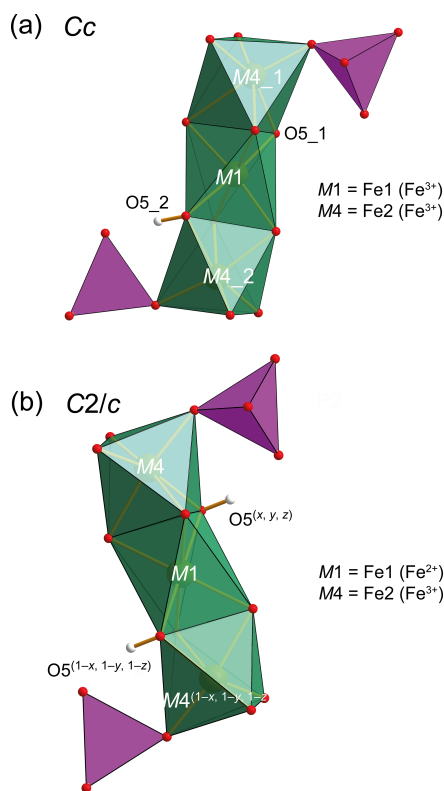


Figure 11. Octahedral trimers in beraunite (a) and ferroberaunite (b). Symmetry operations are given for the centrosymmetric structure. $M1$ is occupied by Fe^{3+} (beraunite) and Fe^{2+} (ferroberaunite). P tetrahedrons are purple and H atoms grey. H atoms in the case of the centrosymmetric structure have a reduced occupancy of 0.5.

ment that beraunite “is typically green, dark blue-green or greenish-grey and is characterized by much lower refractive indices than that of eleonorite”. The first description by Breithaupt (1840) and the character of the original beraunite specimen studied both do not contain evidence for green or dark blue-green beraunite; the same applies to absolutely all samples from the type locality stored in collections of Technische Universität Bergakademie Freiberg and of the National Museum in Prague. It is apparent that beraunite from the type locality was formed by direct crystallization and not by oxidation of another mineral (earlier considerations about pseudomorphoses after vivianite were refuted as early as in the 19th century; Frenzel, 1873, Streng, 1881). Re-investigation of the type material of the beraunite from Hrbek Mine proved the identity of beraunite and eleonorite. Based on this study, the mineral eleonorite was discredited.

Looking at the structure refinement of eleonorite provided by Chukanov et al. (2017), we should pay attention to the R values ($R_1 \sim 6\%$) and a suspiciously low GOF (< 1), higher residual density ($1.02 \text{ e } \text{Å}^{-3}$), and the fact that their model has to involve a partially occupied H site (H sites remained undefined in that study). Their model actually in-

cludes the OH1 site considered half O and half OH occupied. All those facts suggest that the structure they present is, in fact, an average structure of the real non-centrosymmetric beraunite structure.

The comparative data for beraunite and related minerals are given in Table 10. To avoid nomenclature duplicity, the structurally related dark-green-colored phosphate that contains Fe^{2+} in $M1$, currently referred to as beraunite, has been recently approved as the new mineral name ferroberaunite (Tvrđý et al., 2021). This mineral was identified in the mid-20th century due to the development of X-ray diffraction in structural mineralogy, i.e., more than a hundred years later than the mineral beraunite was defined (Fron del, 1949; Moore and Kampf, 1992).

Data availability. Crystallographic data for beraunite are available in the Supplement.

Supplement. The supplement related to this article is available online at: <https://doi.org/10.5194/ejm-34-223-2022-supplement>.

Author contributions. LV suggested a research topic and evaluated the EPMA analyses. JS, JP, ZD, JF, RŠ, NVC, and FV analyzed the material (structure determinations were done by JP, EPMA by ZD and LV, PXRD by JS and LV, optical properties by RŠ, Raman spectroscopy by JS and LV, infrared spectroscopy by NVCh, and density measurement by FV). AM provided information on the original material. JT, JS, and LV interpreted the results and wrote the paper.

Competing interests. The contact author has declared that neither they nor their co-authors have any competing interests.

Disclaimer. Publisher’s note: Copernicus Publications remains neutral with regard to jurisdictional claims in published maps and institutional affiliations.

Acknowledgements. The helpful comments of Anthony Kampf, Pietro Vignola, associate editor Cristian Biagioni, and handling chief editor Sergey Krivovichev are greatly appreciated.

Financial support. This work was supported financially by the Ministry of Culture of the Czech Republic (long-term project DKRVO 2019-2023/1.II.d National 50 Museum, 00023272) and by the Grant Agency of the Masaryk University Brno, Czech Republic (project MUNI/A/1387/2018). IR spectroscopy investigation of beraunite-group minerals was carried out in accordance with the state task of the Russian Federation, state registration no. AAAA-A19-119092390076-7. We received financial support from CzechNanoLab Research Infrastructure supported by MEYS CR (LM2018110) for the collection of diffraction data.

Publisher's note: the article processing charges for this publication were not paid by a Russian or Belarusian institution.

Review statement. This paper was edited by Cristian Biagioni and reviewed by Anthony Kampf and Pietro Vignola.

References

- Aksenov, S. M., Chukanov, N. V., Göttlicher, J., Hochleitner, R., Zarubina, E. S., and Rastsvetaeva R. K.: Mn-bearing eleonorite from Hagendorf South pegmatite, Germany, Crystal structure and crystal-chemical relationships with other beraunite-type phosphates, *Z. Kristallogr.*, 233, 469–477, 2018.
- Anthony, J. W., Bideaux, R. A., Bladh, K. W., and Nichols, M. C. (Eds.): *Handbook of Mineralogy*, Vol. IV, Mineral Data Publishing Tucson, Arizona, ISBN 0-9622097-0-8, 2000.
- Bořický, E.: Zur Entwicklungsgeschichte der in dem Schichtencomplex der silurischen Eisensteinlager Böhmen's vorkommenden Minerale, *Sitzungsberichte der Akademie der Wissenschaften, Mathematisch-naturwissenschaftliche Klasse*, 59, 589–620, 1867.
- Breithaupt, A.: Beraunit, ein neues Glied der Phyllit-Ordnung, *J. Prakt. Chem.*, Barth Verlag, Leipzig, 20, 66–67, 1840.
- Breithaupt, A.: *Vollständiges Handbuch der Mineralogie*, Zweiter Band, I. Phyllites, Anhang 5, Beraunit, Arnoldische Buchhandlung, Dresden und Leipzig, 156 pp., 1841.
- Brown, I. D.: *The Chemical Bond in Inorganic Chemistry. The Bond Valence Model*, Oxford University Press, Oxford, ISBN 0-19-850870-0, 2002.
- Brown, I. D. and Shannon, R. D.: Empirical bond-strength–bond-length curves for oxides, *Acta Crystallogr.*, 29, 266–282, 1973.
- Burnham, C. W.: *Lattice constant refinement*, Carnegie Inst Washington Year Book, 61, 132–135, 1962.
- Chukanov, N. V.: *Infrared spectra of mineral species: Extended library*, Springer-Verlag GmbH, Dordrecht Heidelberg New York London, 1716 pp., <https://doi.org/10.1007/978-94-007-7128-4>, 2014.
- Chukanov, N. V. and Chervonnyi, A. D.: *Infrared Spectroscopy of Minerals and Related Compounds*, Springer, Cham Heidelberg Dordrecht New York London, 1109 pp., <https://doi.org/10.1007/978-3-319-25349-7>, 2016.
- Chukanov, N. V., Aksenov, S. M., Rastsvetaeva, R. K., Schäfer, C., Pekov, I. V., Belakovskiy, D. I., Scholz, R., de Oliveira, L. C. A., and Britvin, S. N.: Eleonorite, $\text{Fe}_6^{3+}(\text{PO}_4)_4\text{O}(\text{OH})_4 \cdot 2\text{H}_2\text{O}$: validation as a mineral species and new data, *Mineral. Mag.*, 81, 61–76, 2017.
- Fanfani, L. and Zanazzi, P. F.: The Crystal Structure of Beraunite, *Acta Crystallogr.*, 22, 173–181, 1967.
- Frenzel, A.: Beraunit, *Neues Jahrbuch für Mineralogie, Geol. Paläontol.*, 23–25, 1873.
- Fron del, C.: The dufrenite problem, *Am. Mineral.*, 34, 513–540, 1949.
- Frost, R.L., López, A., Scholz, R., Xi, Y., and Lana, C.: The molecular structure of the phosphate mineral beraunite $\text{Fe}^{2+}\text{Fe}_5^{3+}(\text{PO}_4)_4(\text{OH})_5 \cdot 4\text{H}_2\text{O}$, *Spectrochim. Acta Pt. A*, 128, 408–412, 2014.
- Gagné, O. C. and Hawthorne, F. C.: Comprehensive derivation of bond-valence parameters for ion pairs involving oxygen, *Acta Crystallogr.*, 71, 562–578, 2015.
- Hoppe, R.: Effective coordination numbers (ECoN) and mean fictive ionic radii (MEFIR), *Z. Kristallogr.*, 150, 23–52, 1979.
- Kraus, W. and Nolze, G.: POWDER CELL – a program for the representation and manipulation of crystal structures and calculation of the resulting X-ray powder patterns, *J. Appl. Crystallogr.*, 29, 301–303, 1996.
- Moore, P. B.: Basic ferric phosphates: a crystallochemical principle, *Science*, 164, 1063–1064, 1969.
- Moore, P. B.: Crystal chemistry of the basic iron phosphates, *Am. Mineral.*, 55, 135–169, 1970.
- Moore, P. B. and Kampf, A. R.: Beraunite: refinement, comparative crystal chemistry, and selected bond valences, *Z. Kristallogr.*, 201, 263–281, 1992.
- Nies, A.: Strengit, ein neues Mineral, *Neues Jahrb. Geol. P.*, 8–16, 1877.
- Nies, A.: Vorläufiger Bericht über zwei neue Mineralien von der Grube Eleonore am Dünsberg bei Gießen, *Bericht der Oberhessischen Gesellschaft für Natur- und Heilkunde*, 19, 111–113, 1880.
- Ondruš, P.: ZDS – A computer program for analysis of X-ray powder diffraction patterns, *Materials Science Forum*, 133–136, 297–300, EPDIC-2, Trans Tech Publications, Enschede, Switzerland, ISBN 0-87849-661-0, 1993.
- Palache, C., Berman, H., and Frondel, C.: *The System of Mineralogy of James Dwight Dana and Edward Salisbury Dana*, Yale University 1837–1892, Vol. II, 7th edn., John Wiley and Sons, Inc., New York, 1951.
- Pechoušek, J., Jančík, D., Frydrych, J., Navařík, J., and Novák, P.: Setup of Mössbauer Spectrometers at RCPTM, *AIP Conf. Proc.*, 1489, 186–193, 2012.
- Petříček, V., Dušek, M., and Palatinus, L.: Crystallographic computing system Jana2006: general features, *Z. Kristallogr.*, 229, 345–352, 2014.
- Petříček, V., Dušek, M., and Plášil, J.: Crystallographic computing system Jana2006: solution and refinement of twinned structures, *Z. Kristallogr.*, 231, 583–599, 2016.
- Pouchou, J. and Pichoir, F.: “PAP” ($\varphi\rho z$) procedure for improved quantitative microanalysis, in: *Microbeam Analysis*, edited by: Armstrong, J. T., San Francisco Press, San Francisco, 104–106, 1985.
- Rigaku (Oxford Diffraction Ltd.): *CrysAlis CCD and CrysAlis RED*, Rigaku Oxford Diffraction Ltd., Yarnton, Oxfordshire, UK, 2019.
- Sejkora, J., Grey, I. E., Kampf, A. R., Price, J. R., and Čejka, J.: Tvrđýite, $\text{Fe}^{2+}\text{Fe}_2^{3+}\text{Al}_3(\text{PO}_4)_4(\text{OH})_5(\text{OH}_2)_4 \cdot 2\text{H}_2\text{O}$, a new phosphate mineral from Krásno near Horní Slavkov, Czech Republic, *Mineral. Mag.*, 80, 1077–1088, 2016.
- Sheldrick, G. M.: SHELXT – Integrated space-group and crystal-structure determination, *Acta Crystallogr.*, 71, 3–8, 2015.
- Steinmann, J.: *Kákoxen*, Archiv für die Gesamte Naturlehre VIII, Schrag Verlag, Nürnberg, 446 pp., 1826.
- Streng, A.: Ueber die Phosphate von Waldgirmes, *Neues Jahrb. Mineral. Geol. P.*, 101–119, 1881.
- Tvrđý, J., Plášil, J., Sejkora, J., Škoda, R., Vrtiška, L., Dolníček, Z., Petr, M., and Veselovský, F.: Ferroberaunite, *IMA*

- 2021-036, CNMNC Newsletter 63, Mineral. Mag., 85, 910–915, <https://doi.org/10.1180/mgm.2021.74>, 2021.
- Tvrđý, J., Plášil, J., and Škoda, R.: New crystal-chemical data on zincoberaunite from Krásno near Horní Slavkov (Czech Republic), *J. Geosci.*, 65, 45–57, 2020.
- Tvrđý, J., Plášil, J., Vrtiška, L., Sejkora, J., Škoda, R., Dolníček, Z., Petr, M., and Veselovský, F.: Ferroberaunite, $\text{Fe}^{2+}\text{Fe}_5^{3+}(\text{PO}_4)_4(\text{OH})_5 \cdot 6\text{H}_2\text{O}$, a mixed-valence iron member of the beraunite series, from the Gravel Hill mine, Perranzabuloe, Cornwall, *Mineral. Mag.*, <https://doi.org/10.1180/mgm.2022.15>, online first, 2022.
- Velebil, D., Vrtiška, L., and Černý, P.: Důl Hrbek u Zaječova – slavné historické naleziště fosfátů, *Minerál*, 26, 412–421, 2018.
- Žák, T. and Jirásková, Y.: CONFIT: Mössbauer spectra fitting program, *Surf. Interface Anal.*, 38, 710–714, 2006.